http://dx.doi.org/10.1016/j.ijplas.2017.01.004

A constitutive model for metal plastic deformation at micro/meso scale with consideration of grain orientation and its evolution

Abstract

Traditional metal forming theories are not accurate in the analysis of micro/meso scale metal deformation behavior due to the so-called size effect. As the deformation process scales down to micro/meso level, the characteristics of grain orientation and its evolution play an important role in the plastic deformation which leads to the significant size effect.

In this study, the pure copper tensile specimens with different grain sizes were prepared. After that the tensile tests were conducted and the flow stresses were recorded. The flow stress is found to decrease with the increase of grain size. In addition, the specimens with coarse grain show greater scatter in flow stress and higher surface roughness due to the grain orientation effect. Furthermore, the volume fractions for three main grain orientations (<111>,<100> and <110>) were measured by electron backscatter diffraction (EBSD) both before and after the tensile tests. It is revealed that <111> is a stable orientation while the grains with the orientation of <110> tends to rotate to the orientation of <111> after deformation.

Based on the experimental data, a constitutive model with the consideration of grain orientation and its evolution was established to analyze the size effect induced. On the basis of grain heterogeneity, Voronoi tessellation was employed to simulate the polycrystalline aggregate of material. The new constitutive model was applied in the finite element (FE)

simulation to characterize the influences of grain orientation and its evolution on the plastic deformation. The simulated results of flow stress, scatter of data and surface roughness for different grain sizes were revealed to be in accordance with the experimental results, which verifies the applicability of the model established in this work.

Keywords: Grain orientation, micro/meso forming, constitutive model, flow stress.

1. Introduction

With the boosting requirement of mini products, micro metal parts are greatly needed in the modern industries such as electronics, fine chemical engineering and medical engineering. Currently, they can be fabricated by employing a variety of manufacturing processes, such as machining [1], bending [2, 3], stamping [4-6], drawing [7, 8], bulge forming[9, 10], molding [11], forging [12, 13] and forward/backward extrusion [14, 15]. Among them micro/meso scale forming process has become one of the major processes to manufacture the micro-metallic parts due to its significant advantages of high productivity, low cost, satisfying mechanical performance, and near net shape characteristics [16].

As the part geometrical dimensions scales down from macro to micro level [17, 18], the traditional metal forming theories are rendered inefficient in the analysis of micro deformation behaviors due to the so-called size effect. Therefore, the lack of available material model linking different scales limits the utilization of simulation tools in the microforming process affected by the size effect [19]. Accordingly, the precise simulation results of micro/meso forming process are more difficult to acquire than that of conventional forming process.

The size effect originates from two distinctly different sources, i.e. the grain size and the feature/specimen size which involves geometrical scaling of the workpiece. As the forming dimensions decrease from macro to micro/meso scale, the feature size gradually approaches the grain size. Therefore the deformation behaviors of individual grains become more

significant which further leads to the size effect [5, 6].

The reduction of flow stress in micro/meso forming process with the decrease of geometric scale has been extensively investigated [16, 20]. The phenomenon has also been studied analytically by using different models. Among them, Leu [21] established a model by including the size effect given by T/D (sheet thickness/grain size). Kim et al. [22] proposed a grain boundary based model that can quantify the relationship between the grain size and the feature/specimen size. Furthermore, Zeng et al. [23] investigated the tensile properties and established a constitutive model of ultrathin pure titanium foils. Lai et al. [24] also proposed a mixed model to study the material size effect. In addition, Chan et al. [25] studied the interactive effect of grain and specimen sizes on the flow stress by using a grain boundary strengthening model. Moreover, Liu et al. [17] established a constitutive model by combining the surface layer model and the composite model.

The decreasing repeatability and increasing scatter of experimental data have also been reported a lot in the researches of micro/meso scale forming process. Actually, when the specimen size is scaled down to micro/meso scale, the deformation behavior is characterized by the deformation regions with only a few grains. Therefore, the distributions of the grains with different orientations, sizes and shapes have a significant influence on the overall deformation behavior, which leads to the increasing heterogeneity and scatter of experimental data. Chan et al. [26] found the scatter of experimental data and the inhomogeneous deformation becomes more significant with the decreasing ratio of geometry dimension to

grain size in micro-compression tests. Wang et al. [27] developed a finite element (FE) model of the flexible micro-bending process. In that model, the grain geometrical structure is established with Voronoi tessellation to describe the polycrystalline aggregation. In addition, a crystal plasticity model was reported by Fulop et al. [28] to study the forming of ultra-thin sheet based on FE simulation. They reported that the numerical results are able to predict the overall mechanical properties of different grain sizes and sheet thicknesses. Furthermore, Adzima et al.[29] aslo employed the phenomenological modeling approach and the crystal plasticity finite element method (CPFEM) to investigate the size effect.

In general, different researches have revealed that the deformation of metal material in micro/meso scale is no longer uniform due to the variation of grain orientations as the feature size approaches the grain size. As a results the increase of local imperfection, the reduction of repeatability and formability become more significant. In-depth experimental and analytical investigation on the grain-orientation related size effect in the micro/meso forming process is thus critically needed.

In this study, the uniaxial tensile tests of pure copper specimens with different grain sizes were conducted. The grain-orientation parameters for three main grain orientations were measured by electron backscatter diffraction (EBSD) both before and after the tensile test. A constitutive model with the consideration of grain orientation and its evolution was established. The FE investigations were also conducted to simulate the grain structure by Voronoi tessellation. This study aims to create a link between the microstructure and the

macroscopic response of polycrystalline metals. Therefore, this work can provide a fundamental understanding and characterization of the size effect affected polycrystalline deformation in micro/meso forming process.

2. Experimental Investigations

2.1 Specimen Preparation

The sheet metals of T2 pure copper with the thickness of 1.5 mm were employed in the experiments. The as-received material was annealed with recrystalization at three different temperatures of 400, 700 and 900 $°C$ as shown in Table 1 to remove the hardening effect caused by cold rolling and to obtain different grain sizes. The heating and cooling speeds of heat treatment were 10 $°C$ /minute. In addition, the argon atmosphere was adopted to prevent the oxidation of material during the annealing. After the treatment, the samples were etched with a solution of 10 g $FeCl_3$, 30 ml HCl and 120 ml H_2O for about 15 seconds. The micro structures of material under different annealing temperatures are shown in Fig. 1. In addition, the average grain sizes were also calculated according to ASTM-E211. The results are summarized in Table 1.

Table 1 The heat treatment parameters

Temperature (°C)	*Dwelling time (h)*	*Average grain size (μm)*	*Grain size deviation (μm)*
400	1	12	3
700	2	35	8
900	1	180	20

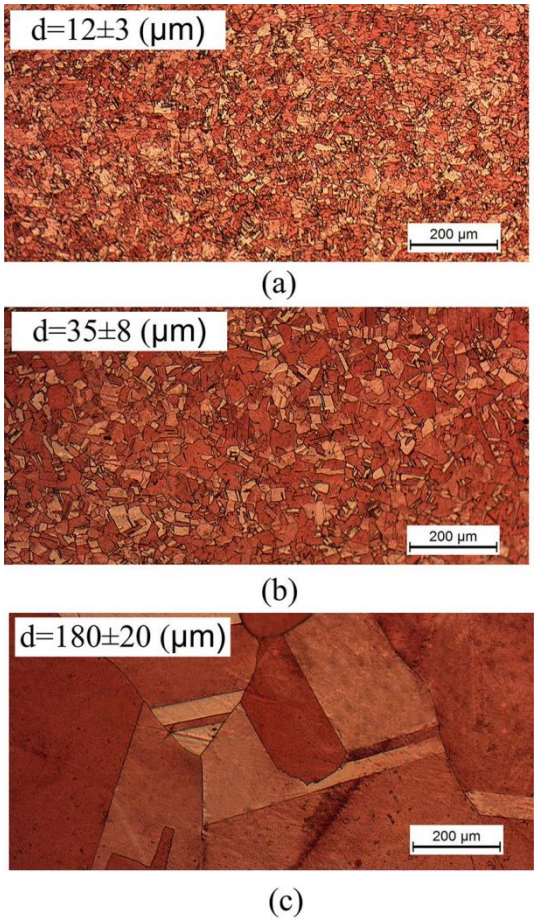

Fig.1 Micro structures of copper samples at different annealing temperatures:

(a) 400 $°C$ (b) 700 $°C$ (c) 900 $°C$

2.2 Tensile Test

The uniaxial tensile experiments were designed according to ASTM-E8. The tensile specimens with the dog-bone shape were prepared by using the wire electric discharge machining (WEDM) process as shown in Fig. 2. The specimens were then tested on a universal testing machine of SUNS-UTM4000 with the moving velocity of 1 mm/min.

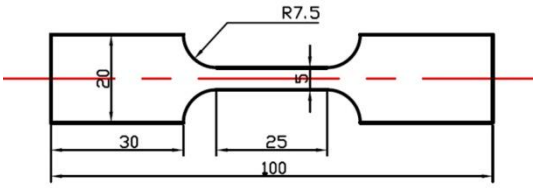

(a)

(b)

Fig. 2 The preparation of specimen:

(a) the geometrical dimensions of design; (b) the fabricated specimen

The flow stress curves of the specimens with different grain sizes are presented in Fig. 3, The mechanical parameters are summarized in Table 2. The significant reduction of flow stress with the increase of grain size can be observed. That can be explained according to the normal Hall-Petch relation presented by Greer and De Hosson [30]. As the grain size increases, the fraction of grain boundary in the unit volume of polycrystalline structure decreases. Considering that the grain boundary impedes the dislocation movement, the strengthening effect of grain boundary thus becomes less significant with the increase of grain size, which leads to the reduction of flow stress.

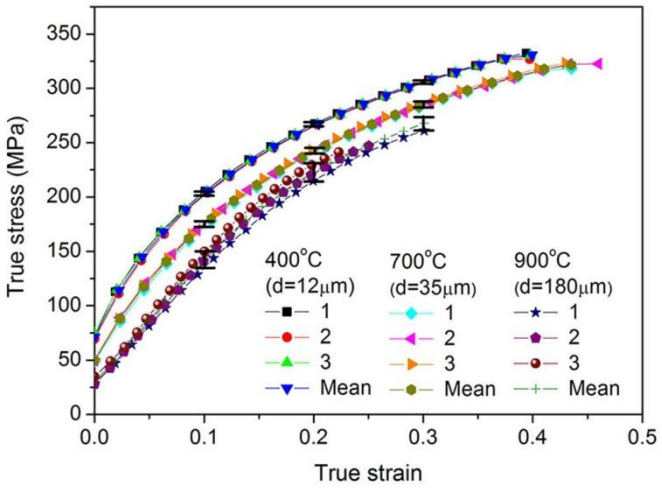

Fig.3 The flow stress curves of material with different grain sizes

Table 2 The mechanical properties of annealed specimens at different temperatures

Temperature (°C)	σ_s (MPa)	σ_b (MPa)	δ (%)
400	72.22	331.27	39.36
700	50.89	323.78	43.22
900	30.54	251.96	27.13

In addition, it can be observed that the percent elongation first increases and then decreases with the increasing grain size. This observation is different from the results reported by Chan and Fu [31]. They found that the percent elongation decreases with the increase of grain size. The reasons for this difference may be attributed to the fact that the as-received material is not fully softened by the complete recrystalization in the 400 $°C$ annealing process. The plasticity of material is thus enhanced by removing the effect of cold working as the annealing temperature increases from 400 to 700 $°C$ which leads to the increase of ductility. However, for the specimens annealed at 900 $°C$ with coarse grains, the uneven deformation of individual grains causes the significant stress concentration at the early stage of

deformation. Therefore, the percent elongation distinctly decreases in that condition.

It can also be noticed that the scatter of experimental data increases with the annealing temperature, indicating that the repeatability of experimental data becomes worse with the increase of grain size. This is because there are fewer grains in the deformation region as the grain size increases. The influence of individual grains on the flow stress thus becomes more prominent with the decrease of grain boundary density. As a consequence, the uneven distribution of individual grains with different sizes, shapes and orientations in the deformation region leads to the significant inhomogeneous deformation and scattered material properties.

The surface microtopgraphy of specimen is also revealed to be affected by the variation of grain size. The KENYENCE VK-X200 laser profile measuring microscope was employed to scan the surface topography both before and after the tensile tests. The sampling position was selected in the homogeneous region of gauge length as indicated in Fig. 4 (a). To verify the repeatability and accuracy of the experimental investigation, three different specimens were tested for each case and three different regions were scanned in each specimen according to ASME B46.1-2009. The results were summarized in Fig. 4 and 5. It can be observed that the surface of specimen is roughened after deformation. In addition, both the surface roughness and its scatter after deformation are revealed to increase significantly with the grain size.

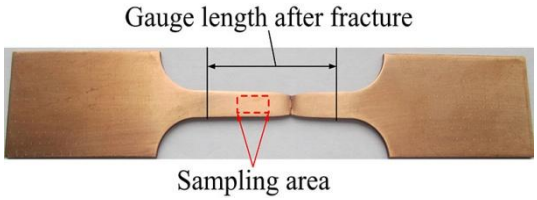

(a)

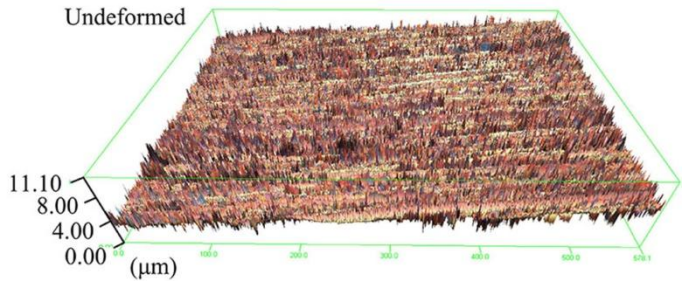

(b)

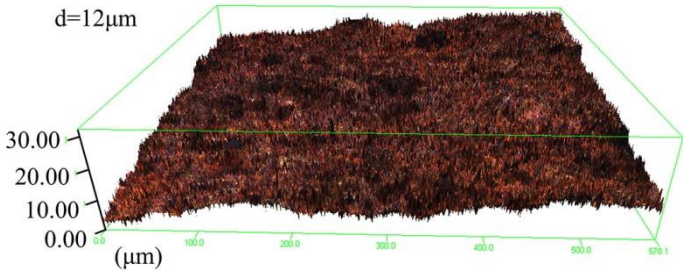

(c)

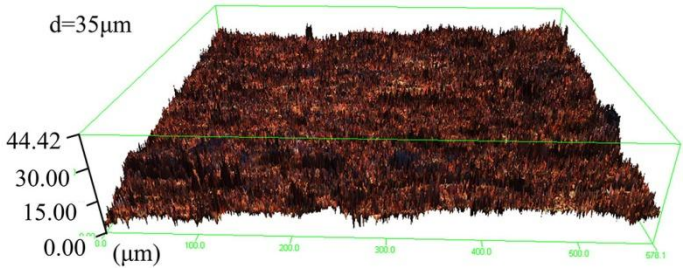

(d)

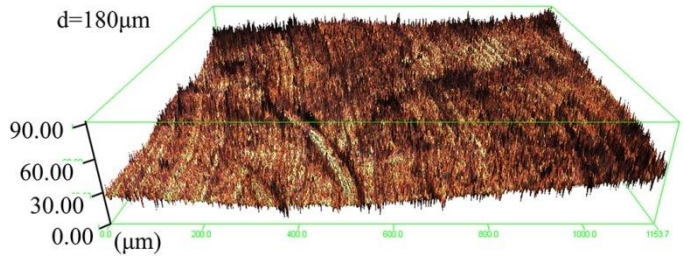

(e)

Fig. 4 Surface microtopgraphies of specimens with different grain sizes before and after

tension:

(a) the sampling area; (b) before deformation;

(c) d = 12 μm ; (d) d = 35 μm ; (e) d = 180 μm

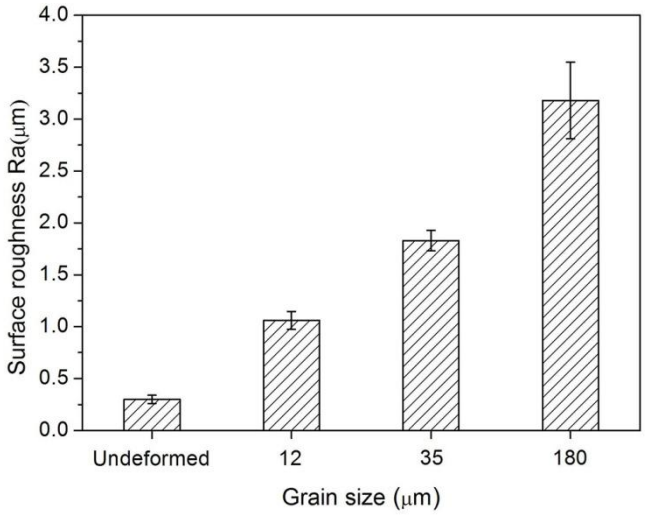

Fig. 5 Effect of grain size on the surface roughness

The reason for the increase of surface roughness with the grain size may attribute to the deformation and rotation of individual grains in the surface layer. Before the grain structure is coarsened, the deformation of individual grain is constrained by each other leading to the overall homogeneous performance of material. With the increase of grain size, the individual grains, especially the surface grains, become less restricted due to the decrease of grain boundary density. Considering that the orientations and structures of individual grains are random distributed, the inhomogeneous and uneven deformations of surface grains become more significant, which leads to the increase of surface roughness with the grain size after tensile test.

2.3 Grain Orientation Detection

The grain orientation and distribution both before and after tensile deformation were detected by using the electron backscattered diffraction (EBSD) process. The samples were first electro-polished in a solution of 125 ml distilled water and 500 ml HPO_3 with the input voltage of 2.1 V for eight minutes at room temperature to obtain high quality surface. After that the detection tests were conducted in the LV UHR FE scanning electron microscope with HKL Channel 5 system. The accelerating voltage is 20 kV and the tilt angle of sample stage is 70 degree. At least 100 grains were investigated in each sampling area and the fraction of successfully-indexed orientation is set as 80%. The orientation image maps (OIMs) of grains before and after deformation along the tensile axis are reconstructed and illustrated in Fig. 6-9. Furthermore, the scattered inverse pole figures are presented in Fig. 10 and the fractions of different grain orientations are summarized in Table 3.

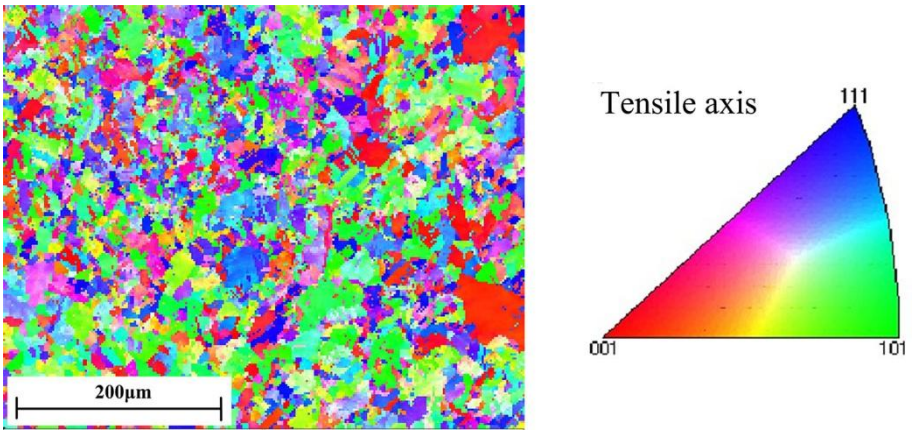

Fig. 6 Grain orientation maps of cold-rolled pure copper before deformation

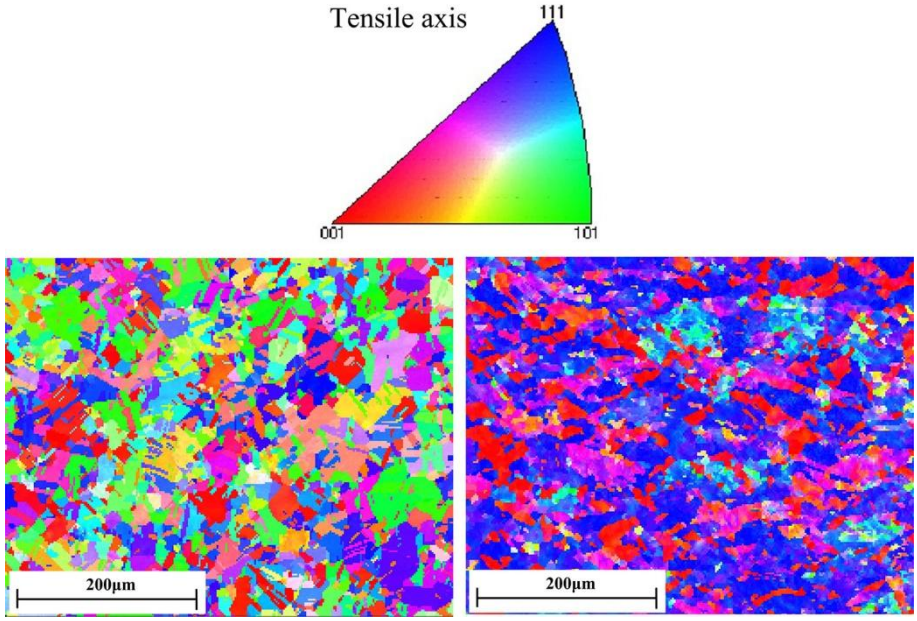

(a) (b)

Fig. 7 Grain orientation maps of copper specimens with the grain size of 12 μm :

(a) before tension; (b) after tension

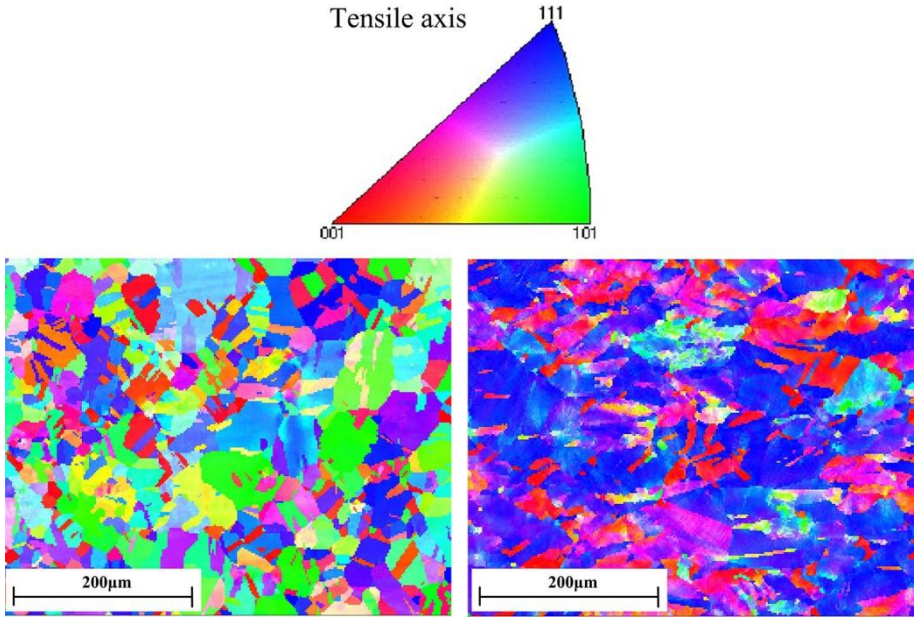

(a) (b)

Fig. 8 Grain orientation maps of copper specimens with the grain size of 35 μm :

(a) before tension; (b) after tension

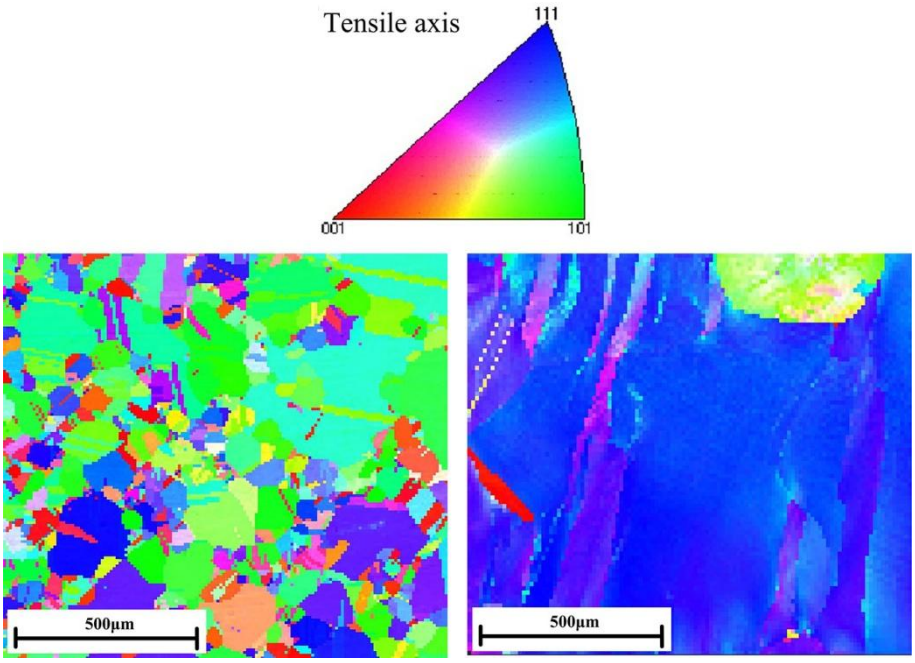

(a) (b)

Fig. 9 Grain orientation maps of copper specimens with the grain size of 180 μm :

(a) before tension; (b) after tension

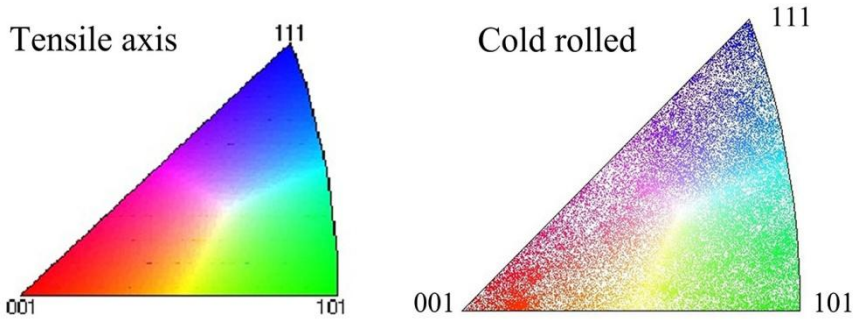

(a)

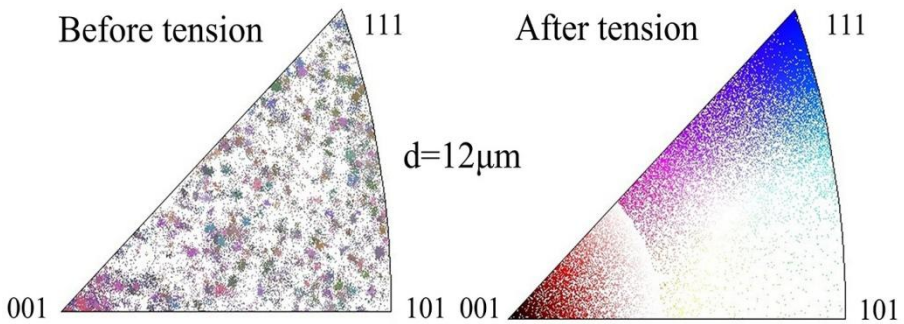

(b)

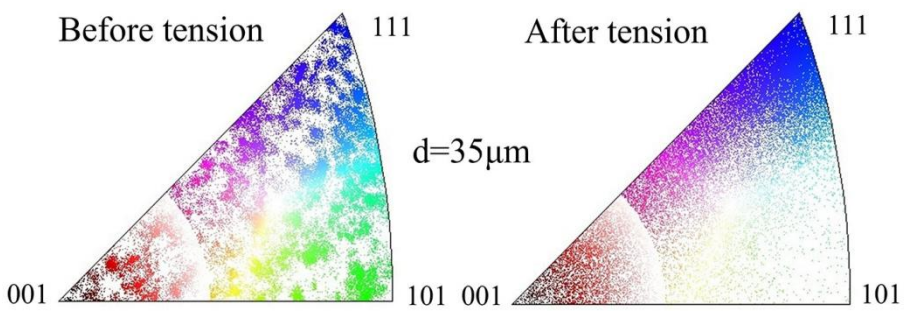

(c)

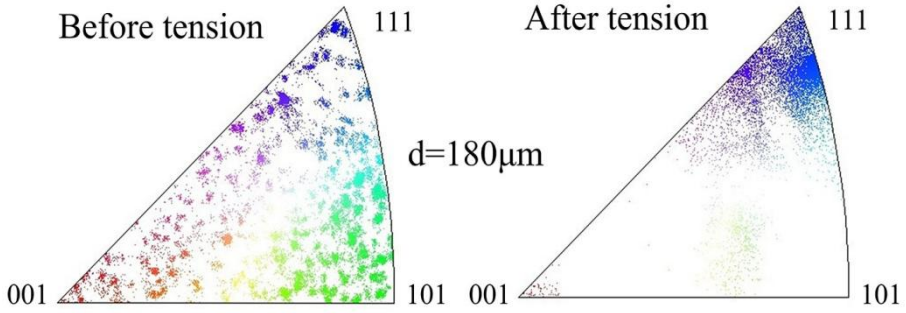

(d)

Fig.10 Scattered inverse pole figures of copper specimens with different grain sizes: (a) as-received; (b) d = 12 μm (c) d = 35 μm (d) d = 180 μm

Table 3 Composition variation of three groups of grains before and after deformation

Grain size (μm)	*State*	*<110>*	*<100>*	*<111>*
12	Before tension	0.35	0.18	0.26
	After tension	0.05	0.21	0.58
35	Before tension	0.42	0.13	0.32
	After tension	0.06	0.15	0.59
180	Before tension	0.58	0.09	0.25
	After tension	0.07	0.01	0.90

In the OIMs of grains, different colors represent the different orientations of grains referring to the roll direction (RD) which is also the tensile axis direction. It can be observed that there

are three main types of grain orientation, i.e. <111>, <110> and <100> . The grains with different orientations are randomly distributed before deformation. The scattered inverse pole figures also show that the crystallographic orientation aggregation is not significant before tensile deformation. According to the OIM results before deformation, the <110> orientated grains take the greatest proportion while the grains with the orientation of <100> take the least for all the three grain size conditions.

After the tensile deformation, it can be observed that the fraction of <110> orientated grains decreases prominently while the fraction of grains with the orientation of <111> increases significantly. On the other hand, the fraction of <100> orientated grains almost remain the same. Hence the <111> and <100> can be considered as the final orientations of grains after tensile deformation. The <111> orientated grains remain in the <111> orientation during the deformation. While the grains with the orientation of <110> tend to subdivide and rotate to the <111> orientation under the action of uniaxial tensile stress. In addition, the orientation of <100> can be treated as a tansitional orientation which remain unchanged during the deformation process. The orientation evolution observation in this study is similar to that from the previous research on the cold drawn experiments of <110>, <100> and <111> orientated single crystal copper [32].

In addition, the orientation factor are also calculated as shown in Table 4. The orientation factor distribution is demonstrated in Fig. 13. The flow stress is revealed to be in direct proportion with the orientation factor according to Taylor's theory. In order to characterize the

effect of grain orientation and its evolution on the flow stress, the results in Table 4 are employed in the modeling process.

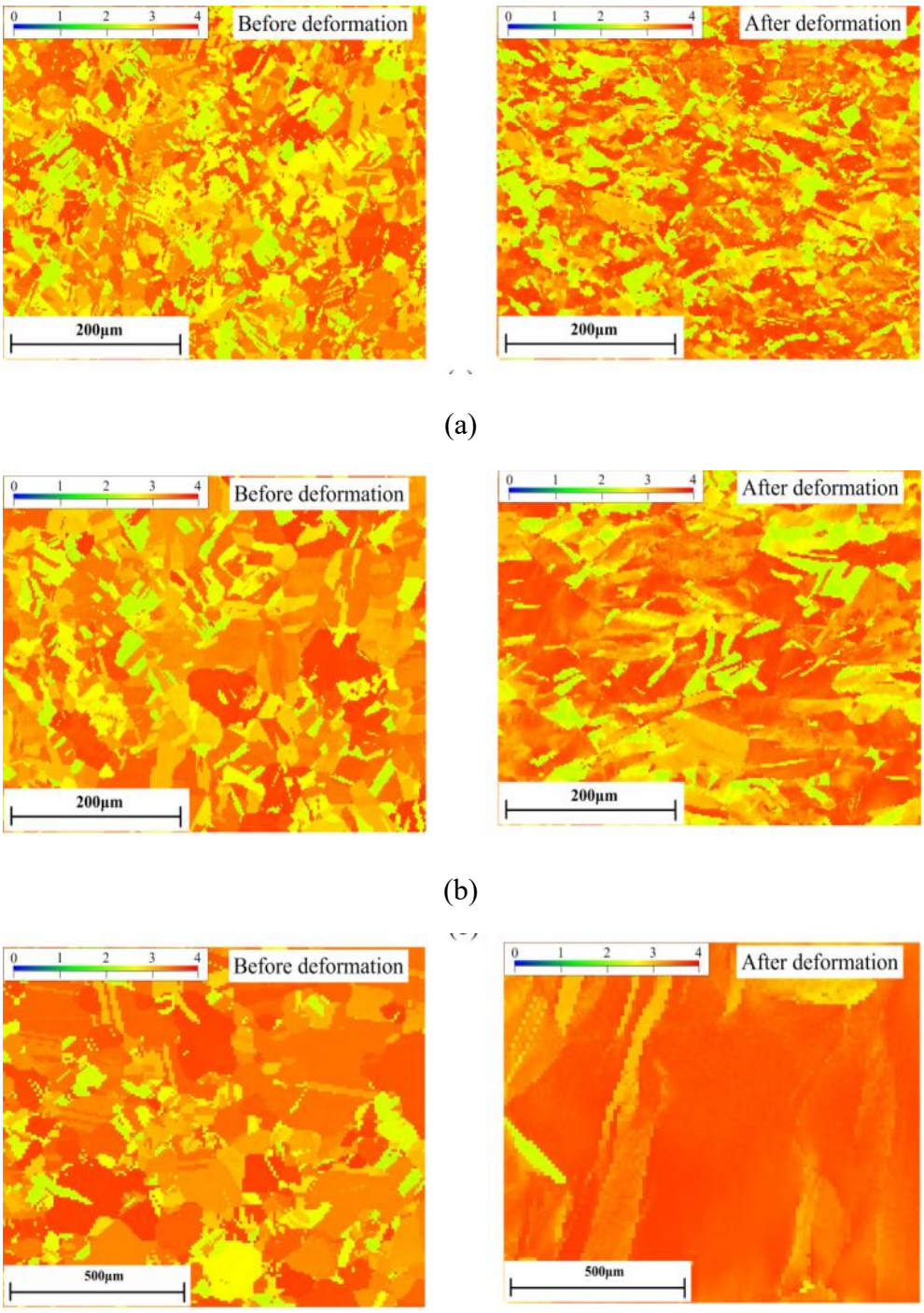

Fig.13 Orientation factor distribution of pure copper specimens:

(a) $d = 12 \ \ \mu m$; (b) $d = 35 \ \ \mu m$; (c) $d = 180 \ \ \mu m$.

Table 4 The measured average grain orientation factors

Orientation	*<110>*	*<100>*	*<111>*
Average factor	3.512	2.418	3.621

3. Constitutive Modeling

In order to characterize the size effect observed in the experimental investigations, a new constitutive modeling method was proposed with the consideration of grain orientation effect.

3.1 Traditional Modeling Method

In macro scale, the Hal-Petch equation is employed a lot to describe the constitutive behavior of polycrystalline material. In the Hall-Petch equation, it is assumed that the normal stress is equal to 2τ , where τ is the resolved shear stress. Therefore the yield stress σ_s can be expressed as follows:

$$\sigma_s = 2\tau_c \tag{1}$$

$$\sigma_s = 2\tau_i + 2kd^{-1/2} \tag{2}$$

If σ_i is equal to $2\tau_i$ and K is equal to $2k$, σ_s may be given as

$$\sigma_s = \sigma_i + Kd^{-1/2} \tag{3}$$

Here, σ_i and K are material constants. Eq. (3) is the Hall-Petch equation derived with the dislocation pileup model [33]. The equation characterizes the relation between the yield stress and the grain size to describe the flow stress for polycrystalline material. According to Eq. (3), the yield stress of material is composed of the two terms. The first one is the shear stress

required to overcome the friction working on the dislocation along the gliding plane in the grain interior. The second one represents the shear stress required to conquer the resistance generated by the dislocation pileup near the grain boundary.

According to Taylor's theory, the yield stress can be expressed by the average orientation factor. The resolved shear stress σ_s can thus be further written as Eq. (4):

$$\sigma_s = M\tau' + MK'd^{-\frac{1}{2}} = M(\tau' + K'd^{-\frac{1}{2}}) \tag{4}$$

In Eq. (4), M is the Taylor factor. The value of M can be variable for different grain structures or orientations. According to Taylor's theory, M equals to 3.1 for the metal material with FCC crystal structure.

Furthermore, Armstrong expanded the Hall-Petch equation into the whole range of flow stress [34-36]. The flow stress of polycrystalline material can be expressed as follows:

$$\sigma(\varepsilon) = \sigma_i(\varepsilon) + K(\varepsilon)d^{-1/2} \tag{5}$$

In Eq. (5), $\sigma_i(\varepsilon)$ and $K(\varepsilon)$ are material constants at the given strain, which reflect the contributions of single grain and grain boundary to the flow stress respectively. Therefore $\sigma_i(\varepsilon)$ can be decomposed as the shear stress of single grain:

$$\sigma_i(\varepsilon) = \tau_i(\varepsilon)(\cos\lambda\cos\phi)^{-1} = M\tau_i(\varepsilon) \tag{6}$$

3.2 Constitutive Model with Orientation Effect

The polycrystalline material can be treated as the aggregate of many randomly-distributed

grains with different orientations. Therefore, the properties of material are determined by the collective function of every individual grain. In macro scale, there are a number of grains located in the section of the material. Although the orientations and shapes of these grains are stochastically distributed, the material demonstrates the overall isotropy properties as the average performance of these grains. As illustrated in Fig. 11, the grain size becomes closer to the feature size as the deformation scale decreases to micro/meso level. As a result, there are only a few grains in the deformation section. Therefore, the orientation and shape of each individual grain play a more significant role in the overall performance of material. In addition, the grains, especially the surface ones, are also less constrained by each other due to the reduction of grain number. The collective material behavior thus performs higher uncertainty due to the random properties of individual grains. This is the intrinsic reason for the size effect of flow stress and surface roughness observed in the above experiments.

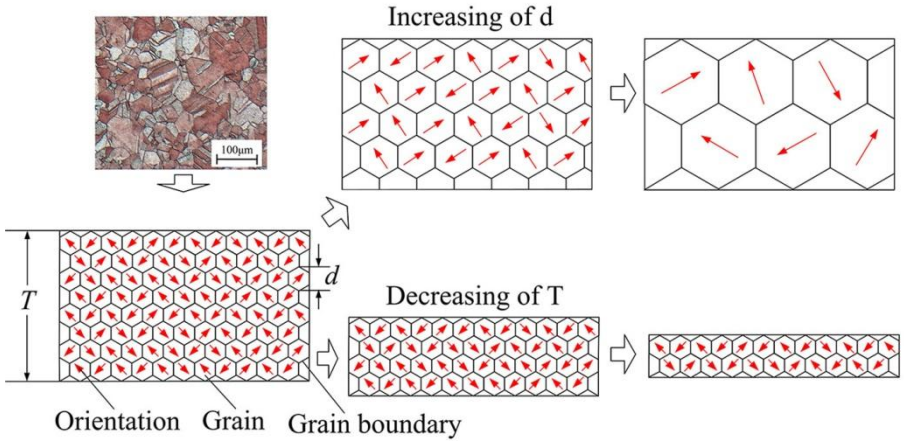

Fig.11 Schematic description of the grain orientation effect

In order to describe this effect, the traditional constitutive method can be modified by considering the collective contribution of each individual grain with different shape, size and orientation. The contribution of each grain is weighted according to the fraction f_i in the

polycrystalline material. Therefore, the total flow stress of specimen can be obtained as follows:

$$\sigma=\sum_{i=1}^{n} f_i M_i(\tau'_i + K_i' d^{-1/2}) \tag{7}$$

In Eq. (7), the overall flow stress is considered to be composed of *n* types of grains with different orientations. In this study, three main orientations, i.e., <110>、<100> and <111>. The total flow stress of material can thus be expressed as follows:

$$\sigma = f_1 M_1(\tau'_1 + K_1' d^{-1/2}) + f_2 M_2(\tau'_2 + K_2' d^{-1/2}) + f_3 M_3(\tau'_3 + K_3' d^{-1/2}) \tag{8}$$

Assuming $\tau'_i (i=1,2,3)$ and $K_i'(i=1,2,3)$ follows the power and exponential function of strain, the following equation can be obtained:

$$\sigma = f_1 M_1\left(A_1\varepsilon^{m_1} + B_1\varepsilon^{n_1} d^{-1/2}\right) + f_2 M_2\left(A_2\varepsilon^{m_2} + B_2\varepsilon^{n_2} d^{-1/2}\right) + f_3 M_3\left(A_3\varepsilon^{m_3} + B_3\varepsilon^{n_3} d^{-1/2}\right) \tag{9}$$

In Eq. (9), f_1 and M_1 are the volume fraction and orientation factor of the grains with the orientation of <110> respectively. f_2 and M_2 are the fraction and orientation factor of the grains with the orientation of <100>, respectively. f_3 and M_3 are the fraction and orientation factor of the grains with the orientation of <111>, respectively. $A_i(i=1,2,3)$, $B_i(i=1,2,3)$, $m_i(i=1,2,3)$, and $n_i(i=1,2,3)$ are all material constant.

The fractions of the three orientations are proportionally extrapolated based on the experimental results. The calculated volume fractions are shown in Table 4. According to the EBSD results, the grain orientations are revealed to evolve under the action of external stress. In this study, the fraction of grains with a specific orientation is assumed to follow the linear function of strain during the uniaxial deformation as given below:

$$\begin{cases} f_1(\varepsilon) = f_{1i} + \dfrac{(f_{1f} - f_{1i})}{(\varepsilon_{1f} - \varepsilon_{1i})}\varepsilon \\ f_2(\varepsilon) = f_{2i} + \dfrac{(f_{2f} - f_{2i})}{(\varepsilon_{2f} - \varepsilon_{2i})}\varepsilon \\ f_3(\varepsilon) = f_{3i} + \dfrac{(f_{3f} - f_{3i})}{(\varepsilon_{3f} - \varepsilon_{3i})}\varepsilon \end{cases} \tag{10}$$

In Eq. (10), f_{1i}, f_{2i} and f_{3i} are the fractions of the grains with the orientations of <110>, <100> and <111> before deformation respectively while f_{1f}, f_{2f} and f_{3f} are the fractions after deformation.

Table 4 Volume fraction of grains with different orientations

Grain size (μm)	*State*	*<110>*	*<100>*	*<111>*
12	Before tension	0.44	0.23	0.33
	After tension	0.06	0.25	0.69
35	Before tension	0.48	0.15	0.37
	After tension	0.08	0.19	0.73
180	Before tension	0.63	0.10	0.27
	After tension	0.07	0.007	0.923

4. Model Validation and Discussion

Based on the EBSD results, the established model was applied on the flow stress curves of different grain sizes according to the regression analysis. The fitted results are summarized in Table 5 and Fig. 12. The flow stress curves of grains with the orientations of <111>, <110> and <100> were obtained based on the method in Ref. [37-40]. In addition, the calculated results based on the developed model as well as the ones without considering the grain orientation development are also illustrated in Fig. 12.

Table 4 The fitted results of the established model

A_1	B_1	m_1	n_1	A_2	B_2	m_2	n_2	A_3	B_3	m_3	n_3
101.61	-3.63	0.47	0.44	171.63	2.37	0.45	0	105.61	3.67	0.41	0

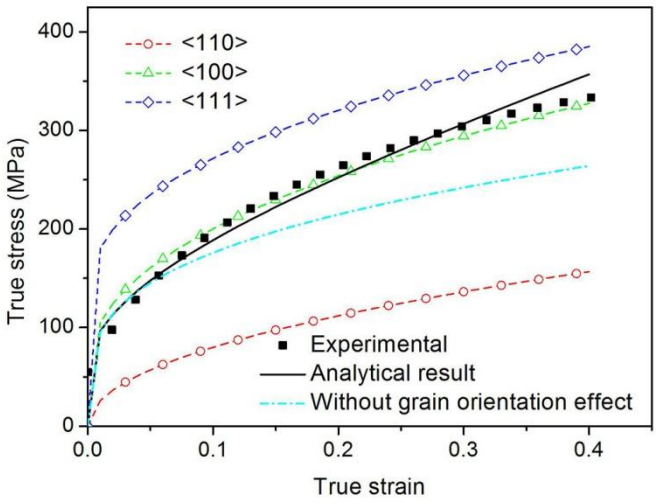

(a)

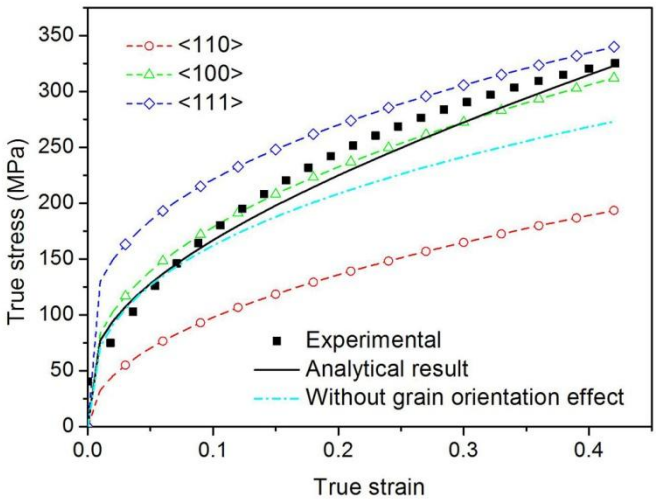

(b)

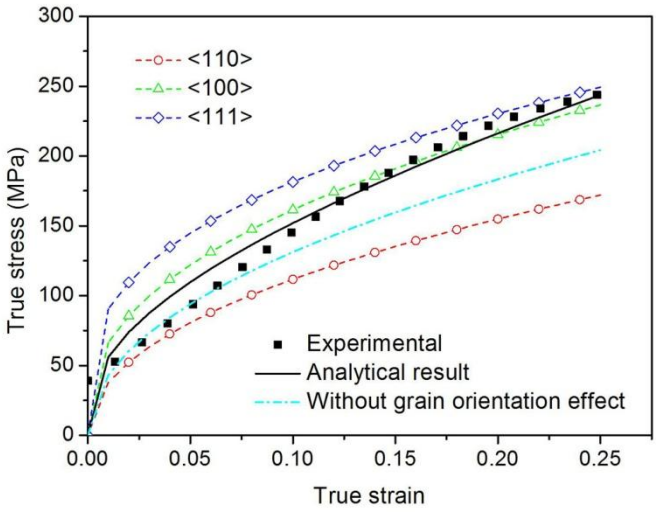

(c)

Fig.12 Comparison of analytical and experimental results:

(a) $d = 12 \ \ \mu m$; (b) $d = 35 \ \ \mu m$; (c) $d = 180 \ \ \mu m$.

It can be observed that the calculated results with the consideration of grain orientation development agree with the experimental results. On the other hand, the calculated results without considering the grain orientation effect are close to the experimental ones at the small strain. However, the difference between the calculated and experimental results increases significantly with the strain. This is because that the grains with the orientation of <110> gradually rotate to the <111> orientation as the strain increases in the experiment. At the beginning of deformation, the fractions of the grains with different orientations are close to the initial condition. However, the differences of fractions become more and more significant as the strain increases. Therefore, the difference between the predicted and the experimental curves becomes more and more significant if the grain orientation effect is not included.

In order to further verify the accuracy of the proposed material model, the FE model of

uniaxial tension was established. The 2D geometrical model of virtual grains was constructed based on the Voronoi theory [41-43] in ABAQUS/CAE environment for the materials with three different grain sizes. The orientations of grains were defined statistically according to the fractions of grains with different orientations. After that the mechanical properties were defined for each grain according to its orientation based on the predictive results obtained from the established model. In addition, three different structures were generated for each grain size condition to verify the repeatability of simulation. The simulation for each structure was repeated for 20 times by using different grain orientation mapping solutions. CPS4R element were employed in the calculation. The developed numerical models are shown in Fig. 13.

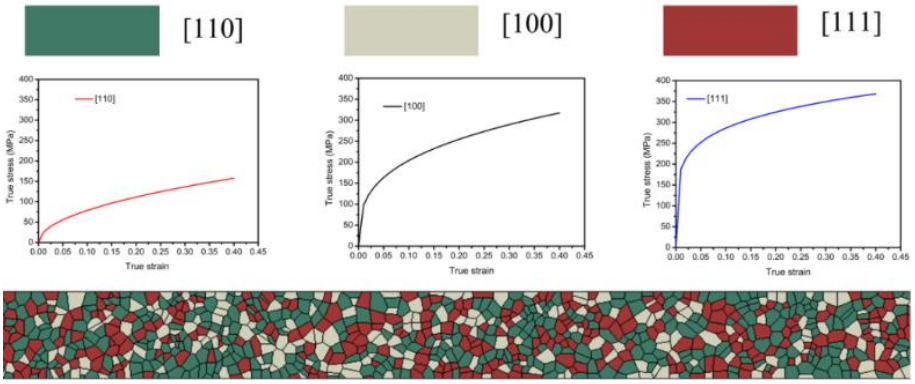

(a)

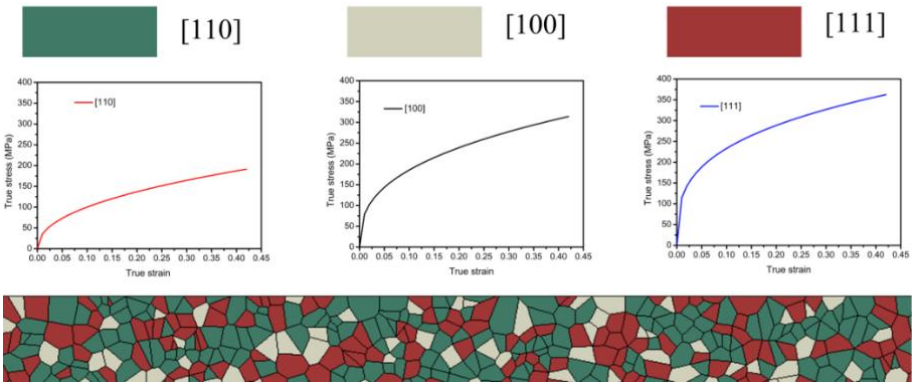

(b)

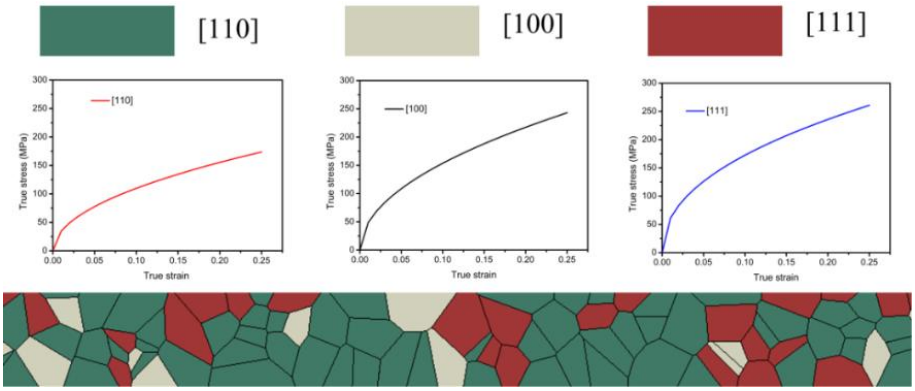

(c)

Fig.13 The FE models of materials with different grain sizes:

(a) $d = 12 \ \mu m$ (b) $d = 35 \ \mu m$ (c) $d = 180 \ \mu m$

The FE results are shown in Fig. 14 (a). The surface roughness for different grain sizes were also calculated based on the FE results. The predicted and the experimental results are both shown in Fig. 14 (b). It can be observed that the FE results agree with the experimental one. Both the average value and the scatter of surface roughness are revealed to increase with the grain size according to the FE results. This is because the mechanical properties of individual grains are different from each other, which leads to the significant inhomogeneous deformation. The uneven deformation can be clearly observed in Fig. 14 (a). As the grain size increases, the number of grains in the deformation area decreases. Therefore the individual grains are less restricted by each other and the inhomogeneous deformation thus become more and more severe. Hence the surface roughness increases as a consequence. The FE simulation thus provides an intuitive and persuasive demonstration of the surface roughness size effect.

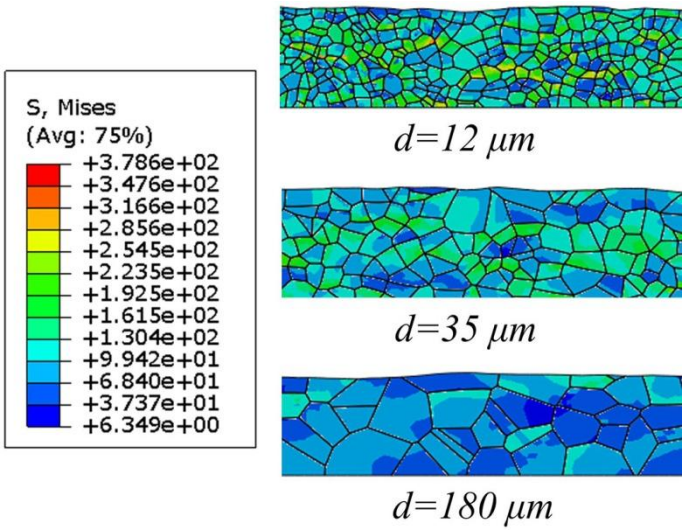

(a)

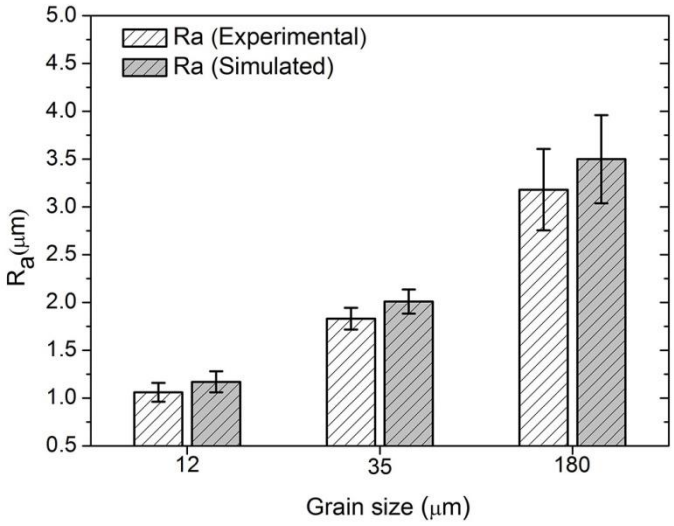

(b)

Fig. 14 Surface topography analysis of the FE results:

(a) The simulated free surface morphology after deformation;

(b) the roughness of deformed surface

The true stress vs. true strain curves for different grain sizes were also obtained as shown in Fig. 15. It can be observed that there is a satisfying agreement between the experimental and simulated results. On the one hand, the simulated average flow stresses agree with the

experimental results under different strain and grain size conditions. On the other, the scatter of simulated results also increases with the grain size, which is in accordance with the experimental observation. This is because the properties of individual grains were defined statistically. The number of grains in the deformation area decreases as the grain size increases. Therefore the overall deformation behavior becomes more dependent on the property and deformation of individual grain. Since the properties of individual grains demonstrate the significant randomness, the scatter of data increases with the grain size. Therefore it can be concluded that the developed model can describe the flow stress affected by the grain orientation effect reasonably under different grain sizes. The size effect affected deformation in micro/meso scale forming processes can be represented and approximated in an intuitive and practical manner by combining this model and FE tools. This work thus provide a basic and effective tool for understanding and analyzing the intrinsic reason of size effect in microforming process.

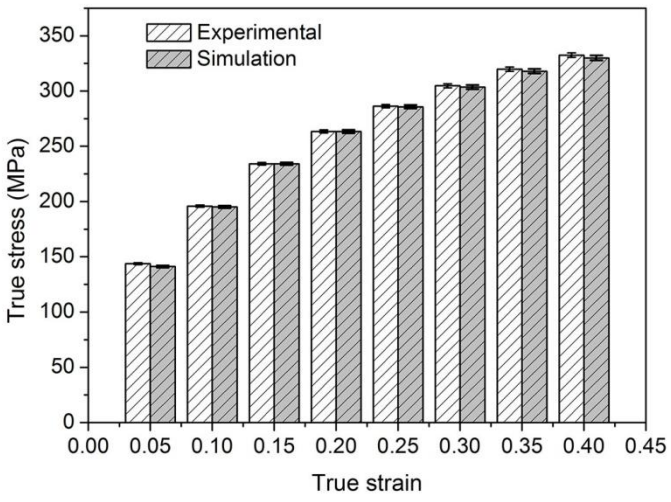

(a)

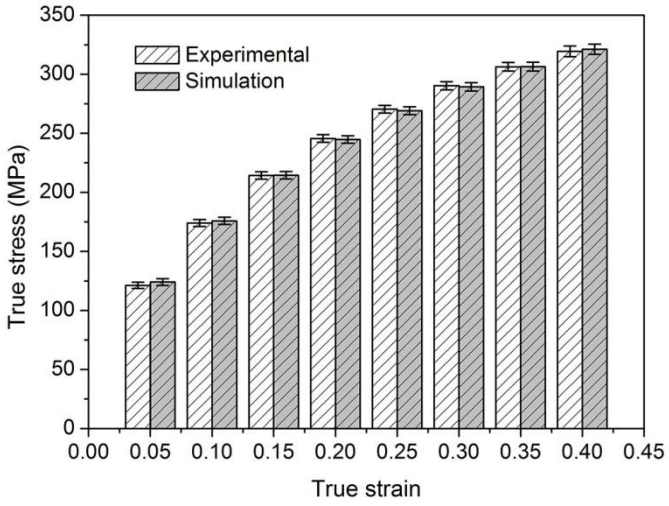

(b)

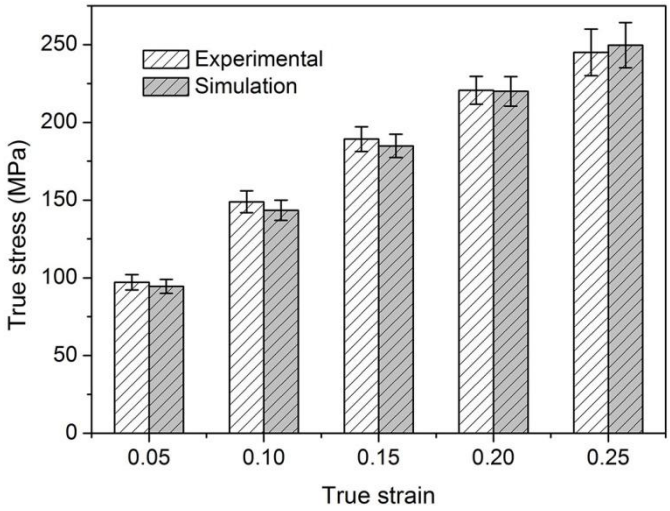

(c)

Fig. 15 Comparison of simulative and experimental results:

(a) d = 12 μm (b) d = 35 μm (c) d = 180 μm

5. Conclusions

The grain orientation and evolution effect on the deformation of copper material at micro/meso scale was investigated by using the uniaxial tensile test. Both EBSD and surface

scanning methods were employed to characterize the grain orientation effect on the micro/meso scale deformation. Based on the discussion, a new constitutive model of flow stress was proposed by considering the grain orientation effect. A Voronoi tessellation based FE method was also employed to simulate the deformation of polycrystalline material and to verify the applicability of the proposed model. The following conclusive remarks can be drawn:

1) The flow stress is revealed to decrease with the increase of grain size according to the experimental results. In addition, the scatter of data and surface roughness were found to increase with the grain size. The inhomogeneous deformation of individual grains was attributed to the phenomenon.
2) EBSD tests of copper specimens were conducted both before and after the tensile test. The grains with the orientation of <110> were identified to rotate to the <111> orientation significantly after deformation.
3) A constitutive model of flow stress was established based on the Hall-Petch equation by including the effect of grain orientation and its evolution. The predicted results were verified by experimental results. The grain orientation effect is revealed to have a significant influence on the flow stress.
4) The FE model of material with different grain sizes was established based on the Voronoi method. By combining with the proposed constitutive model, the predictive results of flow stress and surface roughness are revealed to agree with the experimental results. The effect of grain orientation and its evolution on the deformation at micro/meso scale is found to be one of the intrinsic reason of size effect. Further researches still need to be conducted to

verify the established method in various microforming conditions.

Acknowledgment

This work was carried out within the projects supported by the National Natural Science Foundation of China (No. 51522506, No. 51235008, No. 51421092).

References

[1] Lai X, Li H, Li C, Lin Z, Ni J. Modelling and analysis of micro scale milling considering size effect, micro cutter edge radius and minimum chip thickness. International Journal of Machine Tools and Manufacture. 2008;48:1-14.

[2] Liu JG, Fu MW, Lu J, Chan WL. Influence of size effect on the springback of sheet metal foils in micro-bending. Comp Mater Sci. 2011;50:2604-14.

[3] Chen CC, Jiang CP. Grain Size Effect in the Micro-V-Bending Process of Thin Metal Sheets. Mater Manuf Process. 2011;26:78-83.

[4] Peng X, Qin Y, Balendra R. Analysis of laser-heating methods for micro-parts stamping applications. J Mater Process Tech. 2004;150:84-91.

[5] Peng LF, Hu P, Lai XM, Mei DQ, Ni J. Investigation of micro/meso sheet soft punch stamping process - simulation and experiments. Mater Design. 2009;30:783-90.

[6] Xu J, Guo B, Wang C, Shan D. Blanking clearance and grain size effects on micro deformation behavior and fracture in micro-blanking of brass foil. Int J Mach Tool Manu.

2012;60:27-34.

[7] Gong F, Guo B, Wang C, Shan D. Micro deep drawing of micro cups by using DLC film coated blank holders and dies. Diam Relat Mater. 2011;20:196-200.

[8] Molotnikov A, Lapovok R, Gu CF, Davies CHJ, Estrin Y. Size effects in micro cup drawing. Materials Science and Engineering: A. 2012;550:312-9.

[9] Kim J, Golle R, Hoffmann H. Investigation of size effects of very thin aluminum and copper sheets using aero-bulge test. Mat Sci Eng a-Struct. 2010;527:7220-4.

[10] Mahabunphachai S, Koc M. Investigation of size effects on material behavior of thin sheet metals using hydraulic bulge testing at micro/meso-scales. Int J Mach Tool Manu. 2008;48:1014-29.

[11] Attia UM, Alcock JR. Fabrication of hollow, 3D, micro-scale metallic structures by micro-powder injection moulding. J Mater Process Tech. 2012;212:2148-53.

[12] Bai Y, Yang M. Investigation on mechanism of metal foil surface finishing with vibration-assisted micro-forging. J Mater Process Tech. 2013;213:330-6.

[13] Fu MW, Chan WL. Micro-scaled progressive forming of bulk micropart via directly using sheet metals. Mater Design. 2013;49:774-83.

[14] Cao J, Krishnan N, Wang Z, Lu H, Liu WK, Swanson A. Microforming: Experimental Investigation of the Extrusion Process for Micropins and its Numerical Simulation Using RKEM. Journal of Manufacturing Science and Engineering. 2004;126:642-52.

[15] Chan WL, Fu MW, Yang B. Study of size effect in micro-extrusion process of pure copper. Materials & Design. 2011;32:3772-82.

[16] Peng L, Yi P, Hu P, Lai X, Ni J. Analysis of Micro/Mesoscale Sheet Forming Process by

Strain Gradient Plasticity and Its Characterization of Tool Feature Size Effects. Journal of Micro and Nano-Manufacturing. 2015;3:011006-.

[17] Liu JG, Fu MW, Chan WL. A constitutive model for modeling of the deformation behavior in microforming with a consideration of grain boundary strengthening. Comp Mater Sci. 2012;55:85-94.

[18] Vollertsen F, Biermann D, Hansen HN, Jawahir IS, Kuzman K. Size effects in manufacturing of metallic components. Cirp Ann-Manuf Techn. 2009;58:566-87.

[19] Justinger H, Hirt G. Estimation of grain size and grain orientation influence in microforming processes by Taylor factor considerations. J Mater Process Tech. 2009;209:2111-21.

[20] Fang Z, Jiang ZY, Wang XG, Zhou CL, Wei DB, Liu XH. Grain size effect of thickness/average grain size on mechanical behaviour, fracture mechanism and constitutive model for phosphor bronze foil. Int J Adv Manuf Tech. 2015;79:1905-14.

[21] Leu D-K. Modeling of Size Effect on Tensile Flow Stress of Sheet Metal in Microforming. Journal of Manufacturing Science and Engineering. 2008;131:011002-.

[22] Kim GY, Ni J, Koc M. Modeling of the size effects on the behavior of metals in microscale deformation processes. J Manuf Sci E-T Asme. 2007;129:470-6.

[23] Zheng Q, Shimizu T, Shiratori T, Yang M. Tensile properties and constitutive model of ultrathin pure titanium foils at elevated temperatures in microforming assisted by resistance heating method. Mater Design. 2014;63:389-97.

[24] Lai XM, Peng LF, Hu P, Lan SH, Ni J. Material behavior modelling in micro/meso-scale forming process with considering size/scale effects. Comp Mater Sci. 2008;43:1003-9.

[25] Chan WL, Fu MW. Experimental studies and numerical modeling of the specimen and grain size effects on the flow stress of sheet metal in microforming. Materials Science and Engineering: A. 2011;528:7674-83.

[26] Chan W, Fu M, Lu J, Liu J. Modeling of grain size effect on micro deformation behavior in micro-forming of pure copper. Materials Science and Engineering: A. 2010.

[27] Wang X, Qian Q, Shen Z, Li J, Zhang H, Liu H. Numerical simulation of flexible micro-bending processes with consideration of grain structure. Comp Mater Sci. 2015;110:134-43.

[28] Fülöp T, Brekelmans WAM, Geers MGD. Size effects from grain statistics in ultra-thin metal sheets. J Mater Process Tech. 2006;174:233-8.

[29] Zheng Q, Shimizu T, Yang M. Scale effect on springback behavior of pure titanium foils in microbending at elevated temperature. J Mater Process Tech. 2016;230:233-43.

[30] Greer JR, De Hosson JTM. Plasticity in small-sized metallic systems: Intrinsic versus extrinsic size effect. Progress in Materials Science. 2011;56:654-724.

[31] Fu MW, Chan WL. Geometry and grain size effects on the fracture behavior of sheet metal in micro-scale plastic deformation. Mater Design. 2011;32:4738-46.

[32] Chen J, Yan W, Li B, Ma XG, Du XZ, Fan XH. Microstructure and texture evolution of cold drawing < 110 > single crystal copper. Sci China-Technol Sci. 2011;54:1551-9.

[33] Hansen N. Hall–Petch relation and boundary strengthening. Scripta Mater. 2004;51:801-6.

[34] Armstrong R, Codd I, Douthwaite R, Petch N. The plastic deformation of polycrystalline aggregates. Philos Mag. 1962;7:45-58.

[35] Armstrong RW. The influence of polycrystal grain size on several mechanical properties of materials. Metall and Materi Trans. 1970;1:1169-76.

[36] Armstrong RW. The yield and flow stress dependence on polycrystal grain size. Applied Science Publishers, London; 1983.

[37] Suzuki H, Ikeda S, Takeuchi S. Deformation of thin copper crystals. J Phys Soc Jpn. 1956;11:382-93.

[38] Takeuchi T. Work hardening of copper single crystals with multiple glide orientations. Transactions of the Japan Institute of Metals. 1975;16:629-40.

[39] Takeuchi T. Orientation dependence of work hardening of copper single crystals near the [001] axis. J Phys Soc Jpn. 1976;40:741-6.

[40] Takeuchi T. Orientation Dependence of Work Herdening of Copper Single Crystals near the [111] Axis. J Phys Soc Jpn. 1976;41:490-5.

[41] Stoyan D, Kendall WS, Mecke J, Ruschendorf L. Stochastic geometry and its applications: Wiley Chichester; 1995.

[42] Zhu HX, Thorpe SM, Windle AH. The geometrical properties of irregular two-dimensional Voronoi tessellations. Philosophical Magazine A. 2001;81:2765-83.

[43] Okabe A, Boots B, Sugihara K, Chiu SN. Spatial tessellations: concepts and applications of Voronoi diagrams: Wiley. com; 2009.